Supplementary Figures

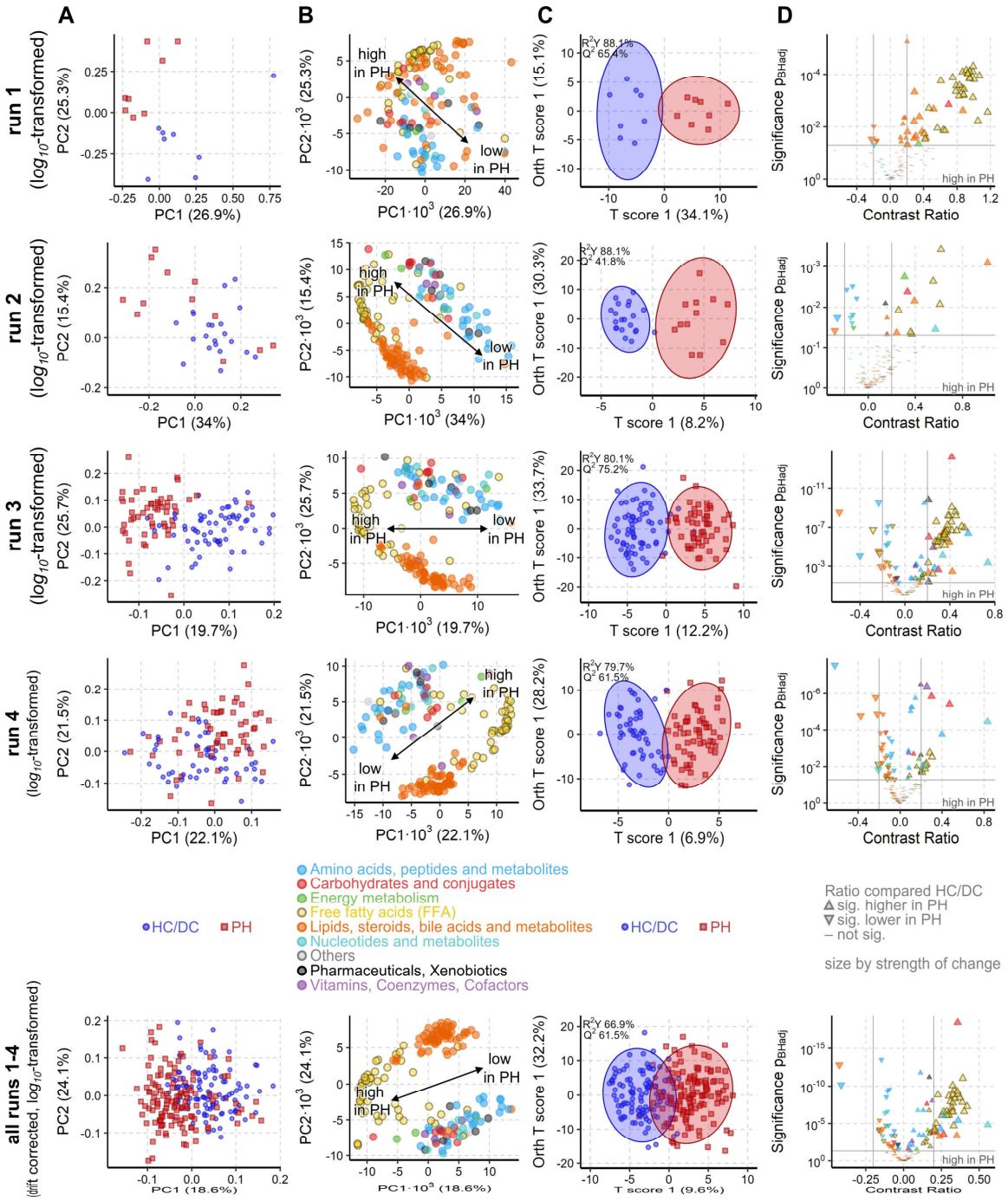

Fig. S1. PH is associated with a strong metabolic shift in every measurement run. (A) iPCA scores plot representing the metabolic profile of each sample as a dot. The proximity of the dots indicates the similarity of the subjects' metabolomes. Clear group separation by PH is visible along the first and or second component for each run and when all runs are jointly analyzed. (B) To A corresponding loadings plot in which each dot represents the contribution of the metabolite to the group separation observed in the scores plot. Free fatty acids (FFA, yellow circles) strongly drive the group separation and are increased in PH patients. (C) OPLS-DA maximizes the group difference from PH to HC/DC and the resulting scores plot represents, as in A, with dots the metabolome of each subjects. Similarly, proximity indicates similarity and ellipses mark the 95% confidence interval of the groups. The difference between the metabolome of PH and HC/DC was significant ($Q^2 > 50\%$, $p < 0.001$). (D) Volcano plot of univariate analysis highlighting significant ($p_{BH} < 0.05$, grey horizontal line) and strong (absolute contrast ratio > 0.25, grey vertical lines) increase in FFAs. For all methods 164 known metabolites and all samples from the measurement run per cohort ($n_1 = 16$, $n_2 = 33$, $n_3 = 118$, $n_4 = 109$) on log_{10}-transformed was used. In run 4 measurement all HC samples from run 3 were repeated to evaluate reproducibility of samples across measurement runs.

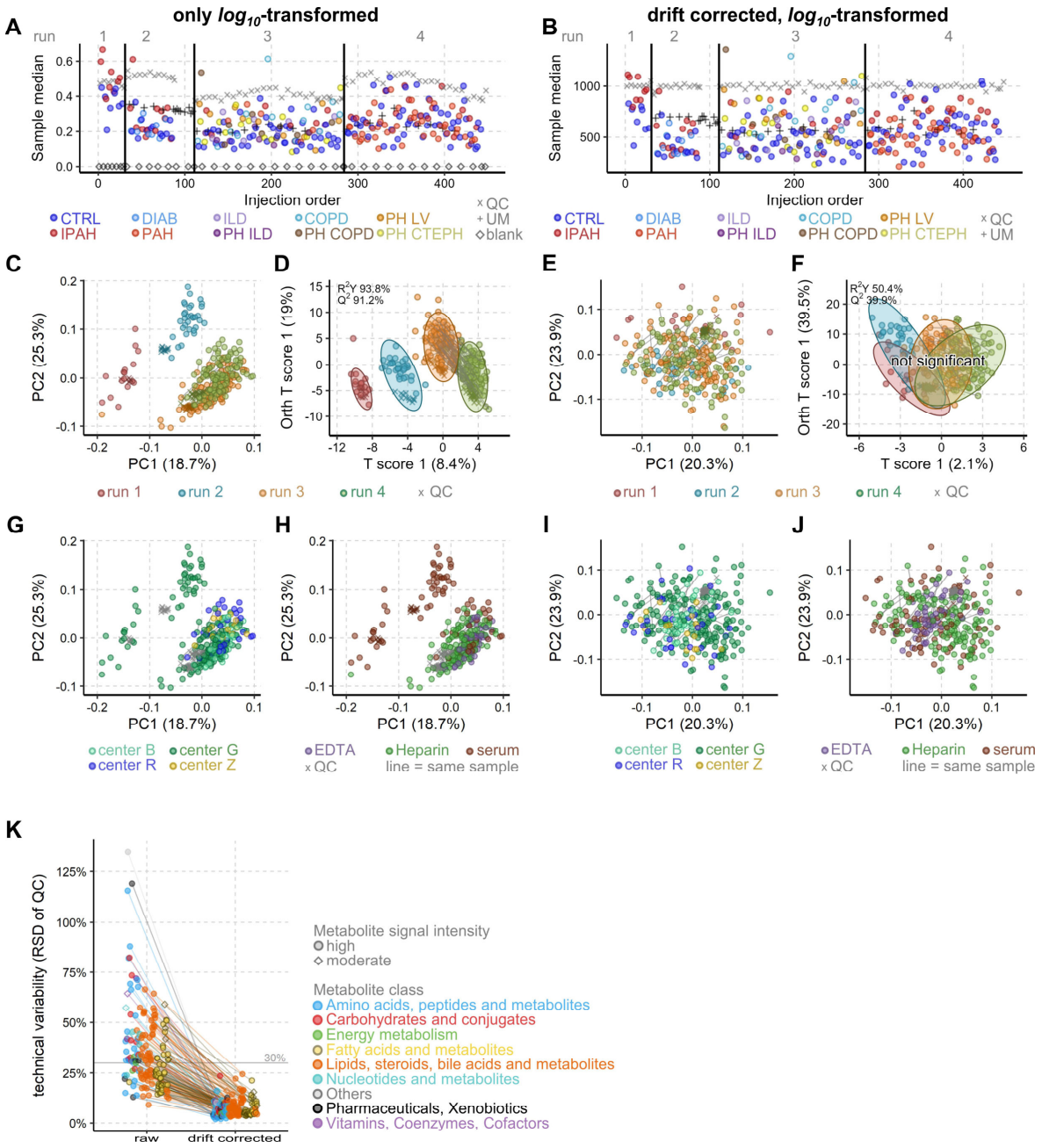

Fig. S2. Drift correction improves data quality enabling a unified analysis of all 4 measurement runs. (A, B) Plot of the sample's median signal intensity of all metabolites versus the sequence of measurement with measurements runs being separated by vertical black lines. **(A)** The QC samples (grey x) fluctuate within each measurement (= drift), while the batch effect is well visible as signal intensity jumps between the measurements. **(B)** Drift correction with an RF-based algorithm on QC samples removed drift and batch effects from the median sample intensity. **(C, E, G, H, I, J)** iPCA scores plots plot representing the metabolic profile of each sample as a dot. The proximity of the dots indicates the similarity of the metabolomes. Lines connect replicate measurements from same samples. Note **(C, G, H)** are the same iPCA model highlighting different biological factors. Analog **(E, I, J)** are the same iPCA model. **(C)** A clear group separation by measurement run is well visible between all 4 runs, with runs 3 and 4 being more similar due to the back to back measurement and shared HC and QC samples. **(D)** Drift correction removes the separation by measurement run. (D, F) OPLS-DA maximizes the differences between runs 1 to 4 and the resulting scores plot represents, as in C, with dots the metabolome of each sample. Similarly, proximity indicates similarity and ellipses mark the 95% confidence interval of the groups. **(D)** All 4 measurement runs were highly significantly ($Q^2 > 50\%$, $p < 0.001$) different before drift correction and **(F)** become non-significant after drift correction. **(G, I)** The observed group separation by sample origin (study center) before drift correction was significantly reduced after drift correction. **(H, J)** The observed group separation by sample material type before drift correction was significantly reduced after drift correction. **(K)** The strong reduction of the technical variability over all 4 runs after drift corrections shows how well the RF-based algorithm reduced technical noise. All plots are based on 164 known metabolites and all samples from the measurement run per cohort ($n_1 = 16$, $n_2 = 33$, $n_3 = 118$, $n_4 = 109$). A, C, D, G, H used *log10*-transformed. B, E, F, I, J used *log10*-transformed, drift corrected data.

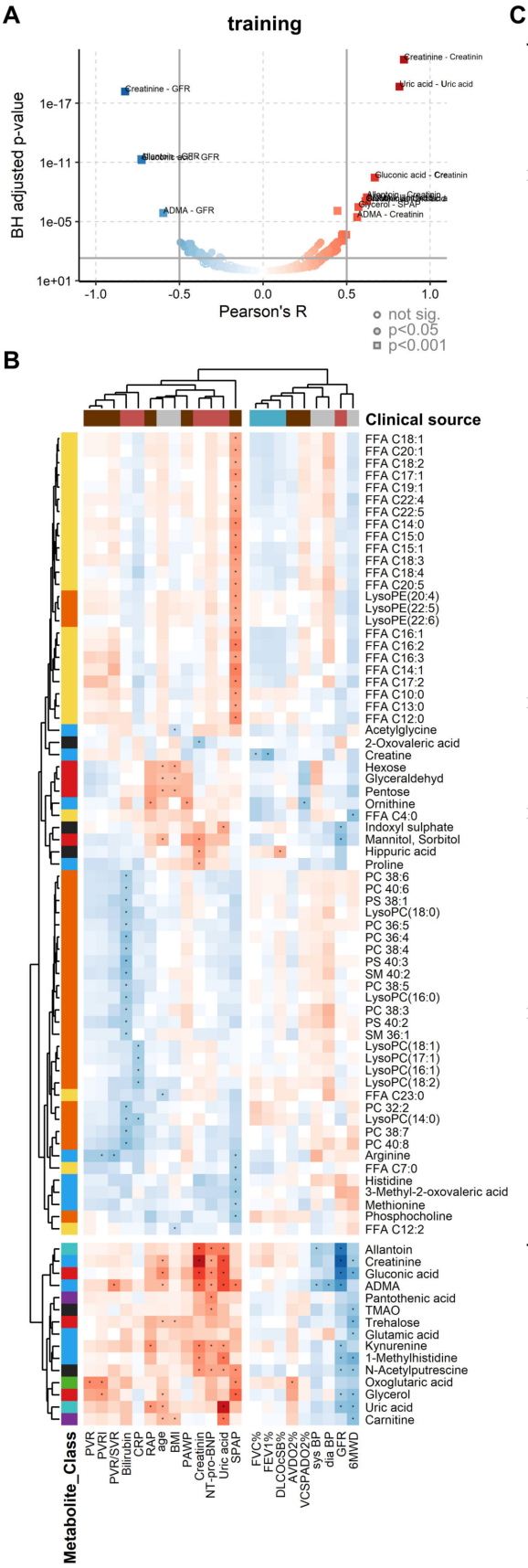

C

	short	description	unit
medical history	age	age at sampling	a (years)
	BMI	body mass index	kg/m²
	6MWD	6-min walk distance	m
	sys BP	systolic blood pressure	mmHg
	dia BP	diastolic blood pressure	mmHg
pulmonary hemodynamics from RHC	mPAP	mean pulmonary arterial pressure	mmHg
	PAWP	pulmonary arterial wedge pressure	mmHg
	CO	cardiac output	L/min
	CI	cardiac index	L/min/m²
	PVR	pulmonary vascular resistance	WU
	RAP	right atrial pressure	mmHg
	PVRI	pulmonary vascular resistance index	WU/m²
	SVR	systemic vascular resistance	WU
	SVRI	systemic vascular resistance index	WU/m²
	PVR/SVR	quotient of PVR/SVR	
	SPAP	systolic pulmonary artery pressure	mmHg
	DPAP	diastolic pulmonary artery pressure	mmHg
	tO2 art%	arterial oxygen content = SaO_2 x K(Hb)	%
	tO2 ven%	venous oxygen content = SaO_2 x K(Hb)	%
	AVDO2%	arterio-venous difference of oxygen = tO2 art% - tO2 ven%	%
	O2	nasal oxygen flow during the assessment	L/min
	SO2%	oxygen saturation	%
	tO2%	oxygen content	%
	VCSPADO2%	vena cava superior - to pulmonary artery - difference in oxygen content	%
blood gas	pO2 art	partial pressure of O_2 in arterial blood	mmHg
	pCO2 art	partial pressure of CO_2 in arterial blood	mmHg
	SO2 art%	arterial oxygen saturation percentage	%
	SO2 ven%	venous oxygen saturation percentage	%
pulmonary function test	FEV1%	% predicted forced expiratory volume 1 s	%
	FVC%	% predicted forced vital capacity	%
	FEV1/FVC%	quotient of FEV1%/FVC%	
	TLC%	% predicted total lung capacity	%
	DLCOcSB %	% predicted single-breath CO diffusing capacity, haemoglobin corrected	%
	DLCOcVA%	% predicted diffusing capacity for CO alveolar volume, haemoglobin corrected	%
haematology	RDW	red cell distribution width	%
	NT-proBNP	N-terminal pro-B-type natriuretic peptide	pg/dL
	Uric acid	uric acid	mg/dL
	Creatinin	creatinine	mg/dL
	Bilirubin	bilirubin total	mg/dL
	Hb	haemoglobin	g/dL
	CRP	C-reactive protein	mg/L
	Albumin	serum albumin	g/dL
	GFR	glomerular filtration rate	mL/min

Fig. S3. Correlation of selected metabolites with clinical parameters in the training cohort. (A) Volcano plot of all pairwise Pearson correlations of all 164 metabolites (drift corrected, *log*$_{10}$-transformed data) versus 43 clinical parameters highlighting strong (absolute R > 0.5, grey vertical lines) and significant (p_{BH} < 0.05, grey horizontal line) correlations. Based on training cohort (n = 169). **(B)** Heatmaps with hierarchical clustering of the respective metabolite vs. clinical parameter. Pearson correlations were filtered to keep only rows and columns with at least

one sig. correlation. All pairwise Pearson correlation results can be found in Supplementary Data 1. Uric acid and creatinine were measured as metabolite and were part of routine hematology. Accordingly, these parameters show the strongest, most significant correlations. **(C)** Overview of all investigated numeric clinical parameters correlated in (A, B) with all metabolites, listing their short names, explanations and units.

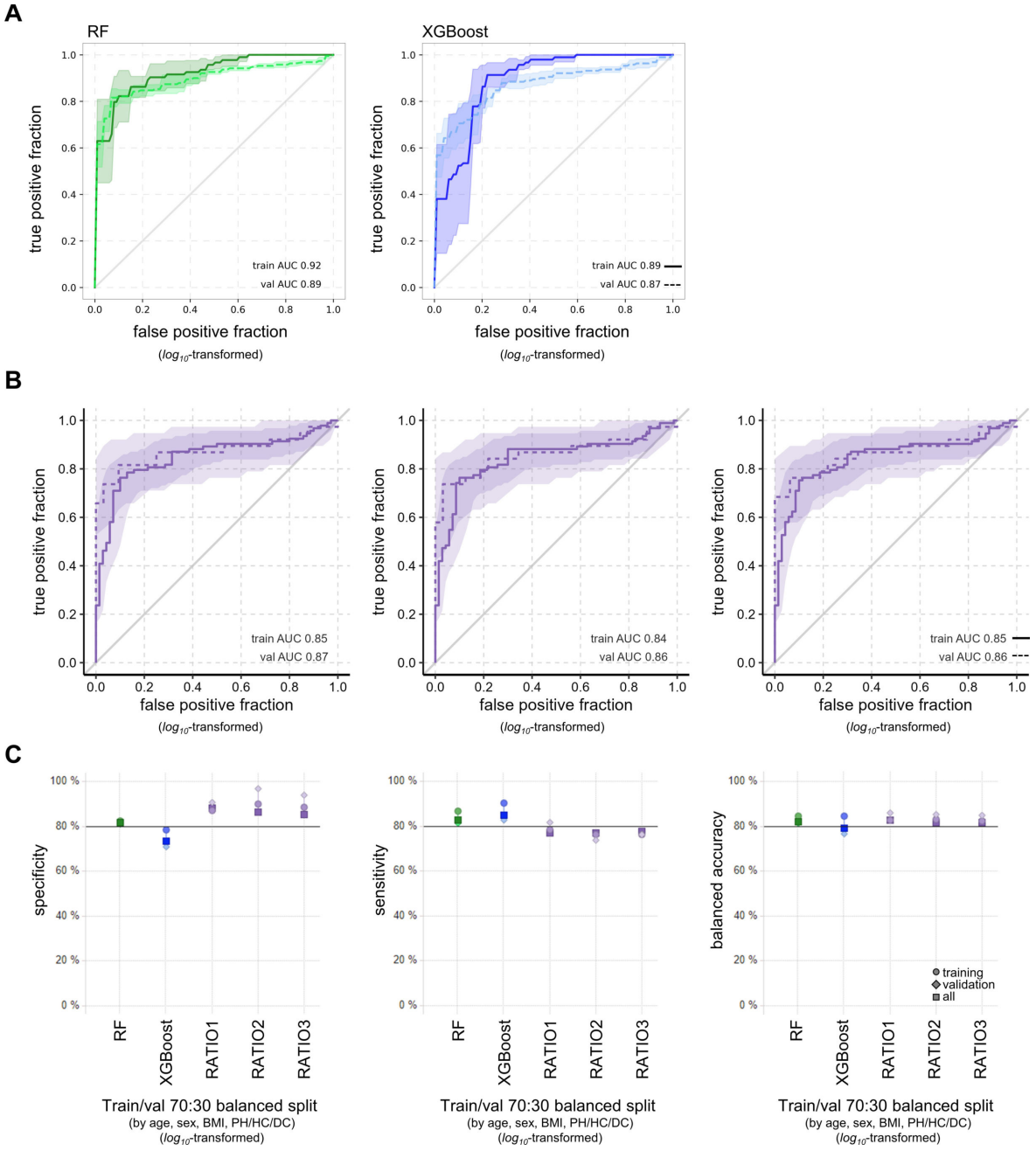

Fig. S4. Data split has little impact on performance of RF, XGBoost or Ratios in predicting PH. The data was split 70:30 into trainings (n = 163, solid line) and validation set (n = 70, dashed line) balanced by age, BMI, sex and class, data was $\log_{10}$-transformed. **(A)** ROC plots of RF (green) and XGBoost (blue) trained with data from training cohort predicting class in validation cohort based on 153 metabolites and 95% confidence intervals marked by ribbons. **(B)** The ROC plots of the three best FFA/lipid-ratios and 95% confidence intervals marked by ribbons. **(C)** Plot of model performance metrics specificity, sensitivity and balanced accuracy for RF, XGBoost, and the three best FFA/lipid-ratios when based on either training (circles) or validation (diamonds) cohorts only or all available data (squares).

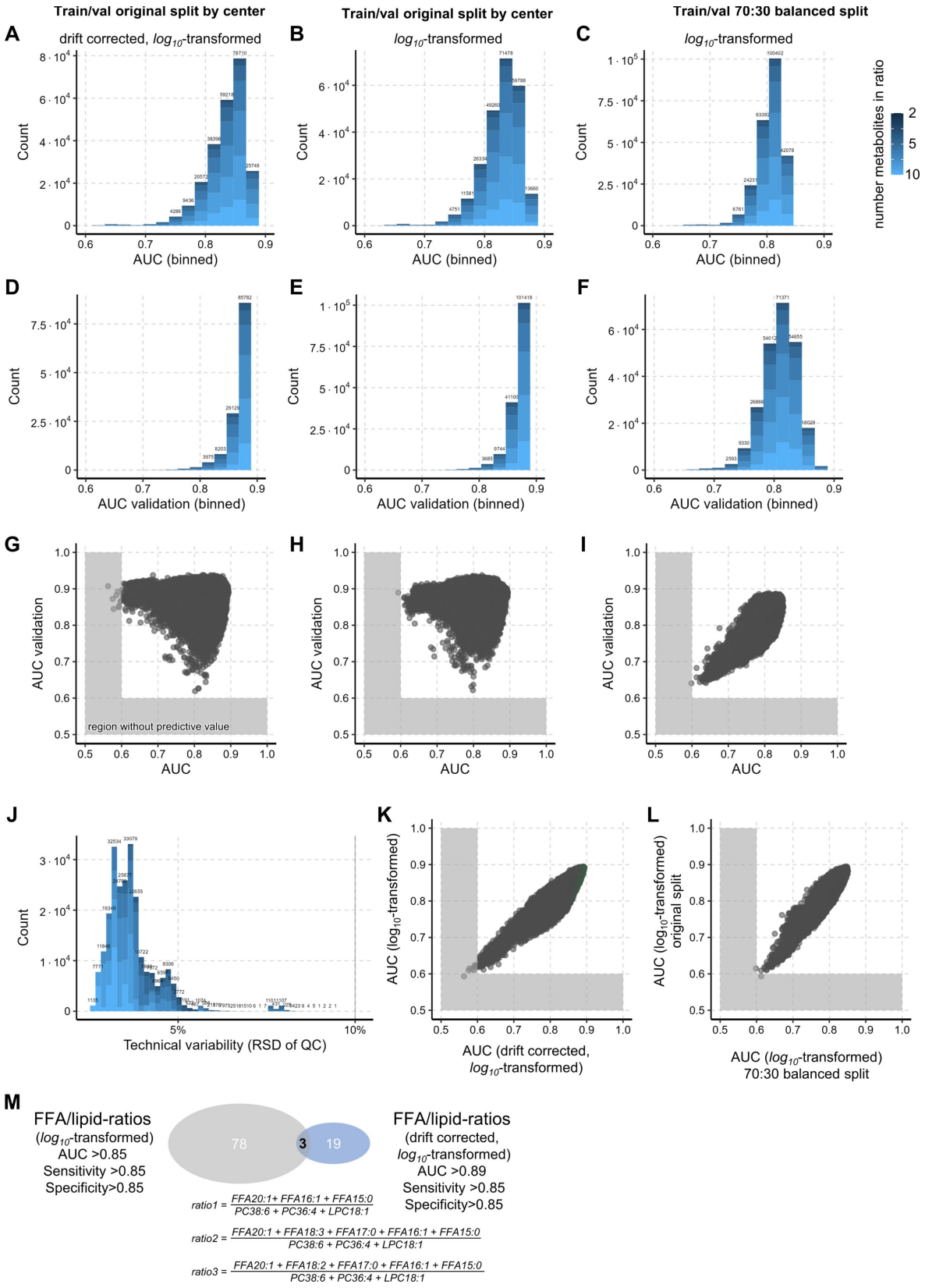

Fig. S5. A quarter million of FFA/lipids-ratios could diagnose PH. (A-F) The histograms summarize the AUCs of the ROC analysis for all 240 570 FFA/lipid-ratios in each data type and split. The histogram of ROC analysis performance AUC for all possible FFA/lipid-ratios exhibits a tight distribution showing that all ratios performed similarly good. **(G-I)** Direct comparison of AUCs between the trainings and validation cohorts. **(A, B, G, H)** ROC analysis within the training cohort (cohort 1, 2, 3 n = 169) of the original split by centers benchmarked against the **(D, E, G, H)** validation cohort (cohort 4 n = 64). **(C, I)** ROC analysis within the trainings set (n = 163) of the 70:30 split (balanced by age, BMI, sex and class PH/DC/HC) and the **(F, I)** validation set (n = 70). **(A, D, G)** are based

on drift log_{10}-transformed, drift corrected data while **(B, C, E, F, H, I)** are based on log_{10}-transformed data. **(J)** The histogram of the calculated technical error ratio for each ratio exhibits a tight distribution around 5% total technical relative variability showing. The grey vertical line marks the maximally acceptable technical variability cut-off for measurement methods in clinical routine laboratories. **(K)** The AUC from **(A)** and **(B)** are very similar to each other, confirming that the drift correction only slightly influences ROC analysis. **(L)** The AUC from **(B)** and **(C)** are very similar to each other, confirming that the split by center delivers very similar results to the 70:30 balanced split. Axes were scaled to exclude empty regions in **(A-I, K, L)**, especially for AUC < 0.6 which have no to very little predictive value. **(M)** Overview of top performing ratios for the original split by center with and without drift correction. The equations for the in both datasets top 3 ratios are given.

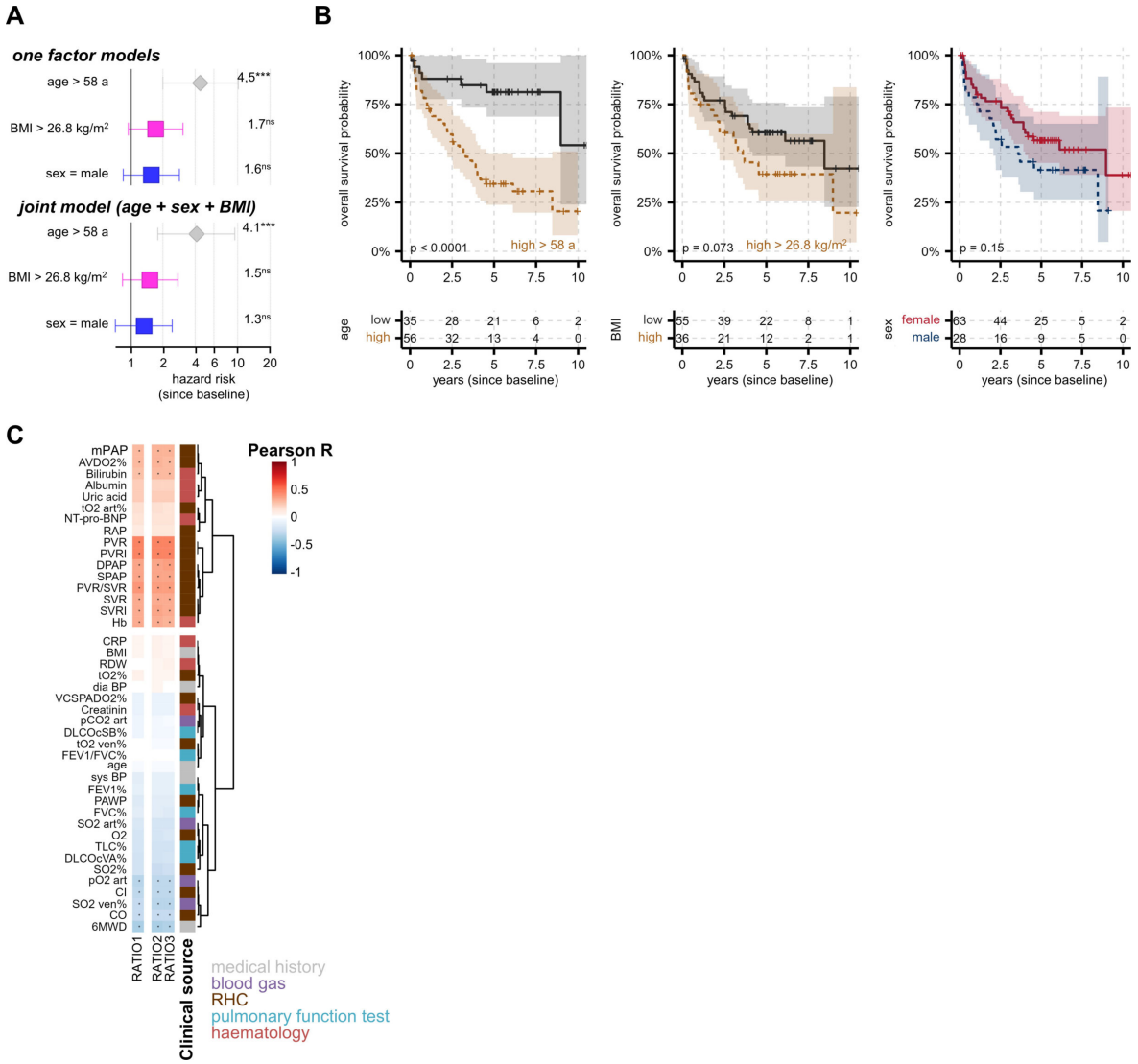

Fig. S6. Survival analysis of covariates age, sex and BMI and linear correlation of top three RATIOs with clinical parameters. **(A)** Cox HR analysis for survival since baseline and the 95% confidence interval with statistical significance coded as not significant (ns); * $p < 0.05$; ** $p < 0.01$; *** $p < 0.001$. Higher age alone and in the tri-factor model was a significant risk factor while BMI and sex were slightly elevated but never significant. **(B)** Kaplan–Meier curves of survival times since baseline by age, sex or BMI. Age and BMI cut-offs were optimized with maxstat. **(C)** Heatmaps with hierarchical clustering of pairwise Pearson correlations of the top three RATIOs (log_{10}-transformed data) versus 43 clinical parameters. All PH patients with survival times and both clinical scores were included (n = 91). All pairwise Pearson correlation results can be found in Supplementary Data 1.

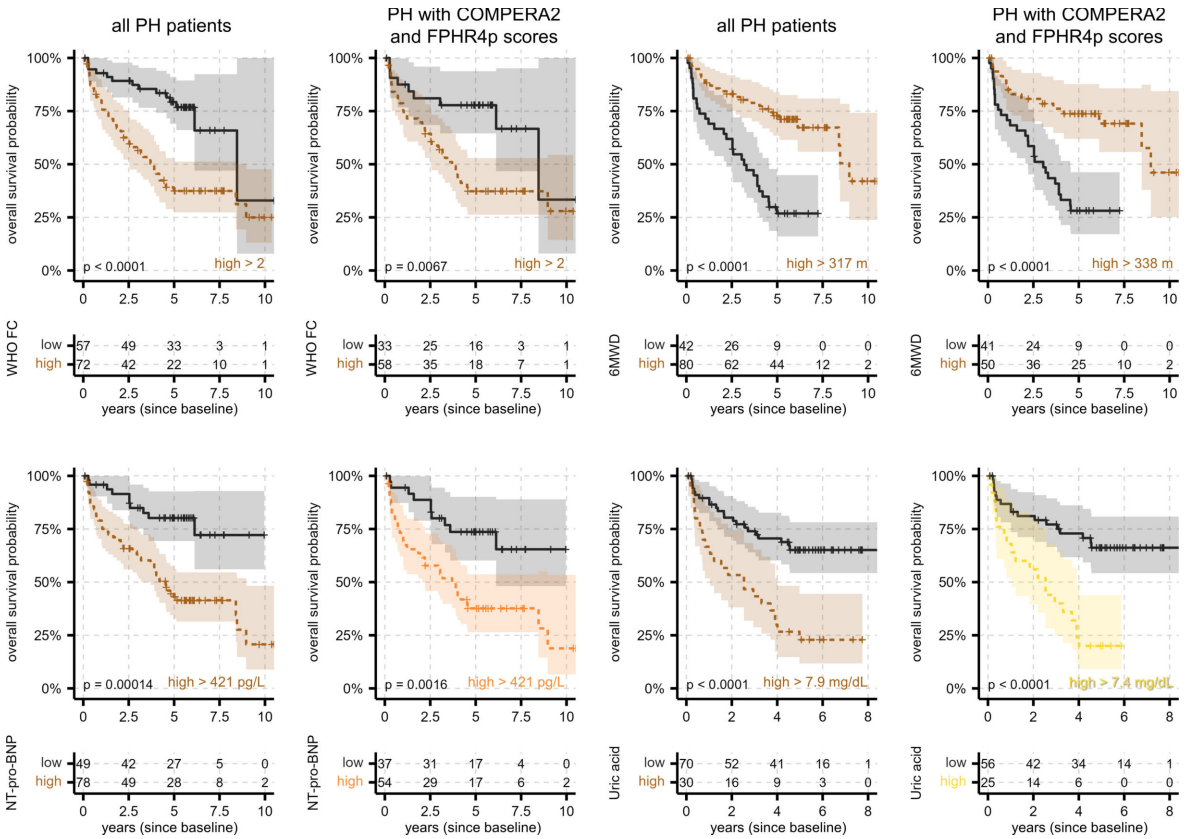

Fig. S7. Survival analysis of established clinical risk factors and top metabolites. Kaplan–Meier curves analyzing survival times since baseline either for all PH patients or PH patients with both clinical scores available (n = 91). The stated cut-off for survival prediction was optimized with maxstat. **(A)** Survival of PH patients significantly decreases with known clinical risk factors such as higher WHO FC classes, lower 6MWD, higher NT-pro-BNP levels, and higher uric acid levels.

442

Supplementary Tables

Table S1: Subject characteristics with medians ± 95% confidence intervals within measurement runs of the training cohort

	run 1		run 2			run 3		
	HC (n=8)	PH (n=8)	HC (n=12)	DC (n=9)	PH (n=12)	HC (n=45)	DC (n=21)	PH (n=52)
Age at sampling, y	57.0±8.8	58.5±9.0	70.5±10.8	56.0±10.1	63.0±9.3	58.0±2.6	60.0±5.7	66.5±3.7
Female:male (ratio)	7:1 (7:1)	7:1 (7:1)	11:1 (11:1)	7:2 (3.5:1)	11:1 (11:1)	26:19 (1.4:1)	13:8 (1.6:1)	30:22 (1.4:1)
BMI kg/m²	22.6±2.7	24.8±3.4	25.8±3.0	30.7±5.5	25.5±3.5	24.1±1.0	22.5±3.2	25.7±1.3
Diagnosis since y	-	3.0±5.9	-	-	6.0±4.0	-	8.0±2.1	0.0±1.1
Pulmonary hemodynamics from RHC								
mPAP (mmHg) mean pulmonary arterial pressure	-	45.0±7.7	-	-	41.5±5.8	-	22.0±0.8[#]	41.0±3.1
PAWP (mmHg) pulmonary arterial wedge pressure	-	10.0±4.2	-	-	5.5±1.7	-	9.5±0.3[#]	10.0±1.6
CO (L/min) cardiac output	-	4.1±1.6	-	-	4.3±0.8	-	3.9±0.4[#]	4.6±0.5
CI (L/min/m²) cardiac index	-	2.3±0.7	-	-	2.5±0.5	-	2.4±0.3[#]	2.6±0.2
PVR (WU) pulmonary vascular resistance	-	8.3±3.7	-	-	8.9±3.1	-	3.2±0.3[#]	6.0±1.2
RAP (mmHg) right arterial pressure	-	5.0±3.8	-	-	5.0±2.4	-	5.0±1.1[#]	7.0±1.5
Clinical data								
6MWD (m) 6-min walk distance	-	338±96	-	-	431±149	-	454±50	317±32
WHO FC world health organisation functional class	-	3.0±0.6	-	-	3.0±0.5	-	2.0±0.3	3.0±0.2
FEV1 (% predicted) forced expiration 1 s	-	83.0±16.5	-	-	82.5±12.9	-	51.5±12	68.5±6.7
FVC (% predicted) forced vital capacity	-	90.9±18.0	-	-	97.6±14.8	-	63.8±8.2	78.0±6.5
FEV1/FVC (% predicted)	-	73.3±6.0	-	-	78.3±6.5	-	56.3±10.3	73.2±3.9
TLC (% predicted) total lung capacity	-	95.7±12.5	-	-	103.1±9.4	-	103.0±13.2	92.0±5.2
DLCO cSB (% predicted) single-breath CO diffusing capacity, hemoglobin corrected	-	69.5±8.4	-	-	65.4±9.5	-	49.6±9.6	56.4±8.2
DLCO cVA (% predicted) CO diffusing capacity alveolar volume, hemoglobin corrected	-	74.6±14.1	-	-	60.6±20.8	-	70.0±9.6	71.0±7.8
RDW (%) red cell distribution width	-	15.5±1.1	-	-	14.4±0.9	-	14.0±0.9	15.7±1.0
NT-proBNP (pg/mL)	-	508±1197	-	-	263±1122	-	98±47	1100±1112.2
Uric acid (mg/dL)	-	5.7±1.4	-	-	5.7±1.6	-	5.0±0.6	6.2±0.7
Creatinine (mg/dL)	-	0.92±0.17	-	-	1.02±0.19	-	0.80±0.11	1.04±0.17
Bilirubin total (mg/dL)	-	0.61±0.25	-	-	0.57±0.26	-	0.40±0.16	0.70±0.17

[#]based on 4 patients, not representative

447 **Table S2: Characteristics of patients with IPAH and healthy donors used for laser capture-microdissection of PA.**

	ID	Age	Sex		ID	Age	Sex	mPAP
Donor	1	[50-59]	male	IPAH	1	[30-39]	female	50
	2	[70-79]	female		2	[30-39]	female	88
	3	[50-59]	female		3	[18-29]	female	56
	4	[30-39]	male		4	[18-29]	female	69
	5	[18-29]	female		5	[50-59]	male	66
	6	[50-59]	male		6	[18-29]	male	74
	7	[18-29]	male		7	[50-59]	male	65
	8	[70-79]	female		8	[30-39]	female	69
	9	[50-59]	female		9	[40-49]	male	96
	10	[50-59]	female		10	[18-29]	female	65

448
449 **Table S3: Primers used to assess the expression of listed genes.** Gene name, PubMed Nucleotide accession number used
450 for primer design, forward and reverse primer sequences and the size of the PCR product (in bp) 4 are given. All
451 primers were designed so that the PCR product span at least one exon-exon junction.

Gene	Forward primer	Reverse primer	Product size (bp)
SLC25(A5)	GTTGTCGCAGGTGGACTTCT	CCTTACCCTCACAACCTGGC	71
GPAT1	CTGCTAGGGCAGCAGCG	TGCTGGGATGAAAGTTCTTCTGT	108
GPAT2	CTTCCCTTGAGCAGTCCACG	GCCATGAGAGCCTCACACCA	87
AGPAT1	ACAGAGACACAGCCATCCG	CAAATCCATTCTGGCCACCTCAG	102
LIPIN2	TCTCCGCCTTCCACAGAGAA	CTGCTTAGACGGGGCAAACA	98
DGAT1	CAACTACCGTGGCATCCTG	TTCTCCAGAAATAACCGGGC	72

452

453

454 **Table S4: Characteristics of the hPASMC and hPAEC donors used for in vitro studies.**

	ID	Age	Sex		ID	Age	Sex
hPASMC	1	[30-39]	male	hPAEC	1	[50-59]	male
	2	[50-59]	female		2	[40-49]	female
	3	[30-39]	male		3	[50-59]	female
	4	[30-39]	female		4	[50-59]	male
	5	[18-29]	female				
	6	[30-39]	male				

455